Coplanar asymmetric $(e,2e)$ experiments on xenon $4d$ and $5p$ orbitals

L. Avaldi, R. Camilloni, and R. Multari*
Istituto di Metodologie Avanzate Inorganiche del Consiglio Nazionale delle Ricerche, Area della Ricerca di Roma CP10, 00016 Monterotondo Scalo, Italy

G. Stefani
Dipartimento di Fisica, Universitá di Roma "La Sapienza," Roma, Italy

X. Zhang† and H. R. J. Walters
Department of Applied Mathematics and Theoretical Physics, The Queen's University of Belfast, Belfast BT7 1NN, United Kingdom

Colm T. Whelan
Department of Applied Mathematics and Theoretical Physics, University of Cambridge, Silver Street, Cambridge CB3 9EW, United Kingdom
(Received 21 January 1993)

Relative triple-differential cross sections for ionization of Xe $4d$ and $5p$ orbitals have been measured in coplanar asymmetric kinematics. The scattered-electron energy is held at 1000 eV while the ejected-electron energy is changed so as to select energy-loss values ΔE in or out of the region characterized by the giant resonance in the $4d \Longrightarrow \varepsilon f$ channel. The ionization mechanism as well as the interference between the direct and resonant processes have been investigated by varying the momentum transfer in a collision at each ejected-electron energy. Strong interchannel coupling between the $5p$ and $4d$ shells in the region of the giant resonance has been observed in $(e,2e)$ experiments. Distorted-wave-Born-approximation calculations have been compared with the experimental triple-differential cross section and used to guide the discussion.

PACS number(s): 34.80.Dp

I. INTRODUCTION

In the last 20 years the ability of electron-electron coincidence techniques to probe the mechanisms of electron-impact ionization and the structure of valence shells of atoms and molecules has been widely investigated [1–3]. It is now well documented that the impulse approximation holds whenever all the energy and momentum transfer to the target are absorbed by the ejected electron [4,5]. Then, within the framework of the single-particle approximation, the cross section is directly related to the momentum density of the ionized orbital. At the other extreme, when the momentum transfer to the target is small, experiments [2] show that first-order theories in the electron-electron interaction have to be extended in order to account fully for the long-range Coulomb interactions of the free electrons among themselves and with the residual ion. All these investigations have involved outer shells of atoms and molecules.

Recently some studies of inner-shell ionization [6–9] as well as attempts to tackle processes in which either the direct ionization competes with ionization via resonant channels [7,10,11] or simultaneous ionization and excitation of the target occur [12–14] have been reported. Following this line, this paper reports on an investigation of an inner shell of Xe, the $4d$ orbital, by asymmetric $(e,2e)$ experiments.

Xe $4d$ has often been used as a showcase for several characteristic features of atomic inner-shell excitation and ionization [15–17]. These features display both one-electron character directly invoking transitions of $4d$ electrons, for instance the shape resonance [18,19], and many-electron character, for example, interchannel coupling between the $5p$ and $5s$ outer shells and Auger decay of the $4d$ vacancies. All these characteristics have been largely explored by photoexcitation and photoionization studies (see, e.g., Ref. [20] and references cited therein). By contrast, data from electron-impact experiments are lacking [21–23].

In order to investigate the different characteristics mentioned above, $(e,2e)$ experiments have been performed at two different values of the energy loss ΔE, namely $\Delta E \cong 90$ and 170 eV. The former value selects ionizing events in which the resonant channel is expected to play a relevant role, as shown in Fig. 1, where two energy-loss spectra in the region of the $4d$ excitation and ionization ($60 \leq \Delta E \leq 95$ eV) collected at small scattering angles are displayed. The low-energy resolution of these experiments, performed at about 1000-eV incident energy, allows us only to resolve the two main features of the $4d_{5/2,3/2} \Longrightarrow np$ Rydberg series [24] converging to the $4d_{5/2,3/2}$ ionization thresholds. However, above the $4d$ thresholds a large increase of the cross section is observed. Previous photoabsorption [20] and electron-energy-loss [23] experiments have shown that the contribution of the resonant channel is relevant at $\Delta E \cong 90$ eV and negligible at $\Delta E \cong 170$ eV (see Figs. 4 and 7 in Refs. [20] and [23], respectively). Therefore, it is straightfor-

ward to interpret the enhancement observed in Fig. 1 as an effect of the shape resonance.

To investigate possible interchannel coupling between the $4d$ and outer valence shells, $(e,2e)$ measurements of the Xe $5p$ triple-differential cross section (TDCS) have also been made at ΔE values corresponding to ionizing events in and out of the resonance region. At each value of ΔE, for both the $4d$ and $5p$ orbitals, several measurements at different momentum transfers K, from the minimum allowed by the experimental apparatus up to values which fulfil the Bethe ridge conditions, have been made. To guide the discussion of the experimental results, distorted-wave-Born-approximation (DWBA) calculations have been made [25]. The DWBA approximation has described successfully $(e,2e)$ processes on the outer shell of rare gases in coplanar and noncoplanar symmetric geometries [25–28] and also the ionization of inner shells at high incident and ejected electron energies [9].

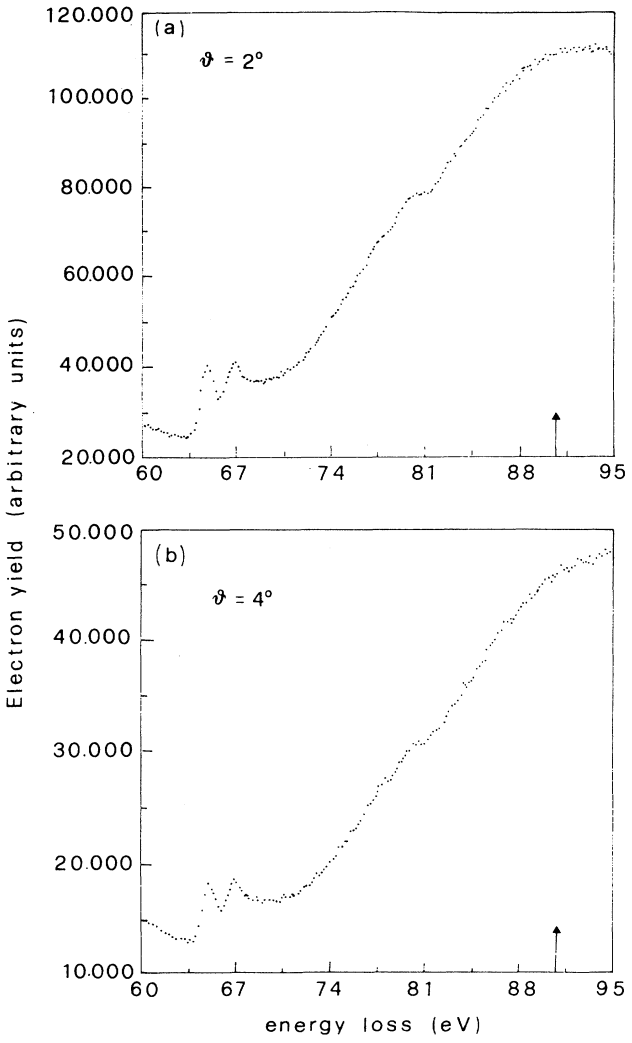

FIG. 1. Energy-loss spectra in the region of the Xe $4d$ excitation and ionization at $\vartheta_a = 2°$ (a) and 4° (b), respectively. In both of the measurements the scattered electron energy is 1000 eV, while the incident energy varies from 1060 and 1095 eV. The arrows show the value of the energy loss $\Delta E = 90$ eV.

II. EXPERIMENT

The apparatus used for the present measurements is an electron-impact spectrometer specially designed for electron coincidence experiments. It consists of a vacuum chamber that contains an electron-beam source, two twin electrostatic analyzers, which are independently rotatable in the scattering plane, and an effusive gaseous beam [29]. The stainless-steel cylindrical vacuum chamber [130-cm outside diameter (o.d.), 80-cm height] is evacuated by two 1500 $l\,s^{-1}$ turbomolecular pumps. The ultimate pressure is 2×10^{-8} Torr; it increases to a few 10^{-6} Torr when the effusive gas beam is operated. The earth's magnetic field is compensated by three pairs of orthogonal square coils with 300-cm-long sides. Along the vertical and north-south directions, where the components of the earth's magnetic field are larger, an extra coil is inserted in between each pair of coils. In this way the residual magnetic field inside the vacuum chamber never exceeds ±6 mG, while in the region of the scattering center, which is located at the center of the chamber, it is smaller than ±2 mG.

The electron beam is formed by a modified Varian glancing incidence electron gun. Its energy is continuously tunable up to 4 KeV and the maximum available current increases with the energy from 10 up to 200 μA. The present measurements were performed at values of the incident-beam current between 0.3 and 0.5 μA.

The divergence of the electron beam is smaller than $\pm10^{-2}$ rad and its diameter at the scattering center is less than 1 mm. The position and intensity of the electron beam can be measured by five small Faraday cups arranged together to give information on total current, direction, and spatial distribution of the electron beam.

The effusive gaseous beam is obtained by letting the gas through a needle, whose tip is placed 1.5 mm below the electron-beam path. The gas density at the electron-beam–gas-beam crossing point can be as high as 5×10^{12} mol cm^{-3}, which means a local pressure 100 times larger than the background pressure.

The density profile of the overlap of the gas and electron beams has been measured by sweeping, in the scattering plane, a well-focused electron beam across the gas beam and detecting the rate of the scattered electrons at 90° as a function of the deflection of the primary beam. This measurement shows that the overlap region between the electron and the gas beam was about 1 mm and that the Faraday cup enables us to monitor the position of the electron beam to better than 0.1 mm Ref. [29]. Measurements of the density profiles, repeated at several scattered ϑ_a and ejected ϑ_b angle settings, enable us to ensure that both the analyzers subtend an identical scattering volume independent of the angular settings.

The electrons which are either scattered inelastically or ejected by the target into a cone around the direction ϑ with respect to the incident beam are analyzed in energy by passing through one of the two twin electron spectrometers, independently movable in the scattering plane

from $-15°$ to 150° with a precision of 0.1°. Due to the wings of the primary electron beam directly entering the analyzer and to secondary electrons and ions backscattered from the electron spectrometer shield towards the scattering center, the minimum scattering angle achievable is 1.5°. A specially designed Faraday cup, combined with the electron spectrometer, minimizes this latter source of noise for scattering angles between 20° and 1.5°.

The electron spectrometers are formed by a decelerating three-element zoom lens followed by a hemispherical electrostatic deflector (105-mm inside diameter, 135-mm o.d.). These zoom lenses are designed so as to keep window and pupil at fixed positions in space while decelerating the electrons by a factor between 33 and $\frac{1}{10}$. The angular acceptancies of the analyzers in the present measurements were set to $\pm 0.5°$ and $\pm 4°$ for the scattered (labeled a in the following) and ejected (labeled b) electron analyzers, respectively.

The energy resolution depends on the retarding (accelerating) ratio of the electron optics, and its best value, achieved for the largest retarding ratio, is $\Delta E/E = 5\times 10^{-4}$ full width at half maximum (FWHM). In the present experiments two different pass energies E_p have been used, namely 100 and 200 eV. At these E_p's the energy resolution in each analyzer was $\Delta E_a = \Delta E_b = 1.1$ and 1.8 eV FWHM, which results in a coincidence energy resolution $\Delta E_c = \sqrt{\Delta E_a^2 + \Delta E_b^2} = 1.6$ and 2.5 eV at $E_p = 100$ and 200 eV, respectively. In Fig. 2 are shown the $(e,2e)$ energy separation spectra for the ionization spectra of Xe $5p$ and $4d$ at $E_p = 100$ eV. In collecting the coincidence angular distribution the energy resolution [30,31] $\Delta E^{-1} = (\Delta E_a^{-2} + \Delta E_b^{-2})^{1/2}$ was 0.8 and 1.3 eV at the two pass energies, respectively.

The uncertainty in the magnitude of the momentum transfer $\mathbf{K} = \mathbf{K}_0 - \mathbf{K}_a$ and in the direction of $\mathbf{K}$, derived from the quoted experimental energy and angular acceptancies, are strongly dependent on the kinematics investigated. In the worst case they can be as large as 25% ($5p$ ionization at $E_b = 20$ eV and $\vartheta_a = 2.5°$) and $\pm 11°$ ($5p$ ionization at $E_b = 80$ eV and $\vartheta_a = 1.5°$).

Pulses from the electron multiplier (Mullard 248BL/01) are processed by a coincidence chain which consists of preamplifiers (Phillips Instrument 6954/50), constant-fraction discriminator (Canberra 2126), delay lines (EGG DB463) and a time-to-amplitude converter (TAC) (Canberra 1443A). An analogous electronic chain is used to pick up any electronic noise in the experimental room. The noise signal is then used to inhibit the TAC. Pulses from the TAC are fed into a computer-aided measurement-and-control (CAMAC) multichannel analyzer (LeCroy 3001-2301) and then stored, together with the pulses from the discriminator of each channel, into an IBM PS2/30 personal computer. Typical time resolution achieved is 5 nsec FWHM. The personal computer is also used to control the experiment via a CAMAC interface (CAEN C111). Beam energy, gas target density, scattering angles, and energies analyzed by the electron spectrometers are automatically monitored by the computer.

The coincidence measurements reported in this paper were collected in asymmetric conditions, i.e., the energy of the scattered electron is larger than the energy of the ejected one. Namely, E_a has been kept fixed at 1000 eV, while three values (100, 80, and 20 eV) have been selected for E_b. The measurements have been performed by collecting the scattered electrons at a fixed angle ϑ_a, while the ejected electron angle ϑ_b is varied from 30° to 150°. The experimental coincident angular correlations are characterized by the presence of two lobes. The first one nearly in the direction of $\mathbf{K}$ is called the binary peak, while the second one, near the opposite direction, is known as the recoil peak.

The collection efficiency of the ejected-electron analyzer has been calibrated on He by measuring the double-differential cross section (DDCS) $d^2\sigma/d\Omega_b dE$, for energies of the ejected electrons equal to the ones actually collected in the $(e,2e)$ experiments. The measured DDCS's are in good agreement with the one "recommended" by Kim [32] at 20 eV and with the previous experimental determination [32] at 80 and 100 eV, where "recommended" DDCS's are not available.

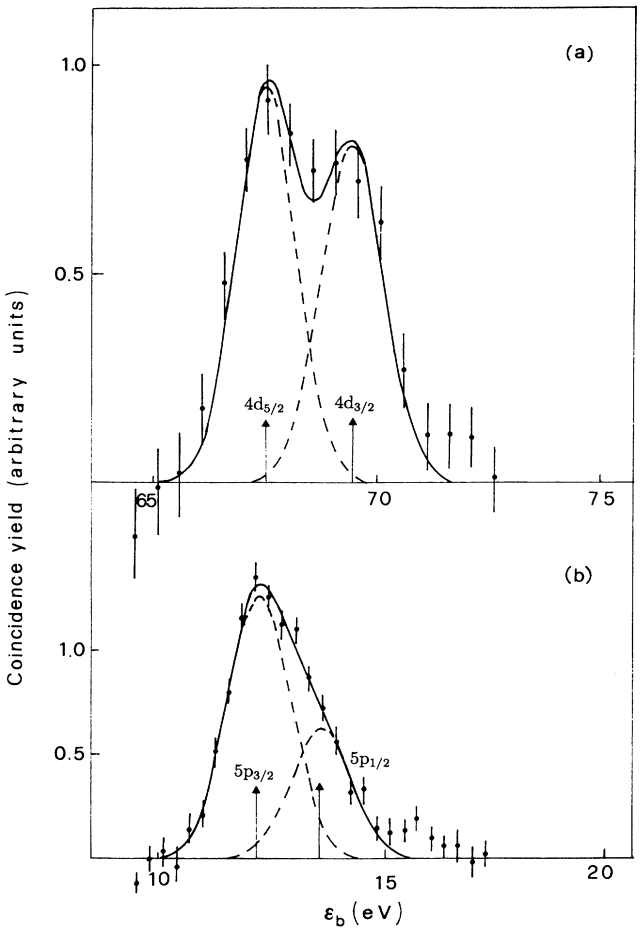

FIG. 2. Xenon $4d$ (a) and $5p$ (b) coincidence transition energy spectra measured at $E_a = 1000$ eV and $E_b = 20$ eV. The angles of the scattering and ejected electrons were 8° and 77° in (a) and 4° and 60° in (b), respectively.

TABLE I. Kinematics of the $(e,2e)$ experiments. ϑ_K is the direction of the momentum transfer $\mathbf{K}$. In the last column the $(\vartheta_a,\vartheta_b)$ pairs (in deg) arbitrarily chosen for the normalization at each ΔE value are reported.

E_a (eV)	E_b (eV)	ϑ_a (deg)	K (a.u.)	ϑ_K (deg)	(θ_a,θ_b)
			Xenon 4*d*		
1000	20	2.0	0.50±0.07	38.0±9.9	
		4.0	0.70±0.09	57.0±4.5	(4,236)
		7.5	1.20±0.10	68.0±1.6	
1000	100	2.0	0.76±0.04	23.0±7.5	(2,70)
		8.0	1.40±0.09	57.0±2.2	
			Xenon 5*p*		
1000	20	2.5	0.40±0.10	68.0±5.3	(2.5,70)
		8.0	1.20±0.10	79.0±0.7	
1000	80	1.5	0.45±0.05	30.0±11.0	
		5.0	0.90±0.10	60.0±3.3	
		12.0	1.90±0.10	72.0±0.8	(12,60)
		15.5	2.40±0.10	73.0±0.6	

The zero of the scattered angle scale was set by determining the symmetry of the scattered-electron DDCS. The full set of kinematics investigated in the present paper is reported in Table I. In this experiment only relative TDCS's have been measured, but each set at fixed ΔE has been internally normalized by a scan in which ϑ_b is kept fixed and ϑ_a moves in the region of interest. The typical coincidence count rate was between 0.02 (Xe 4*d* at $E_b=100$ eV) and 3.5 (Xe 5*p* $E_b=20$ eV), while the true-to-random coincidence was never better than $\frac{1}{3}$. Due to these values the accumulation time in the worse case was about 6 h per point.

III. THEORY

We have performed calculations in the distorted-wave-Born approximation (DWBA). Let $\mathbf{K}_0$ be the momentum of the incident electron and $\mathbf{K}_a$ and $\mathbf{K}_b$ be the momenta of the scattered and ejected electrons in the final state. In the version of the DWBA employed here [34] the triple-differential cross section (TDCS) for ionizing an electron from the (n,l) shell of Xe is given by

$$\frac{d^3\sigma}{d\Omega_a d\Omega_b dE}=2(2\pi)^4\frac{K_aK_b}{K_0}\sum_m [\,|f_{nlm}|^2+|g_{nlm}|^2-\mathrm{Re}(f^*_{nlm}g_{nlm})\,] . \quad (1)$$

Here the sum over m is a sum over the magnetic substates of the (n,l) shell, and $f_{nlm}(\mathbf{K}_a,\mathbf{K}_b)$ and $g_{nlm}(\mathbf{K}_a,\mathbf{K}_b)$ are, respectively, direct and exchange amplitudes for the ionization process. In our approximation these amplitudes are given by

$$f_{nlm}=\langle\chi^-(\mathbf{K}_a,\mathbf{r}_a)\chi^-(\mathbf{K}_b,\mathbf{r}_b)|1/r_{ab}|\chi^+(\mathbf{K}_0,\mathbf{r}_a)\psi_{nlm}(\mathbf{r}_b)\rangle , \quad (2a)$$

$$g_{nlm}=\langle\chi^-(\mathbf{K}_a,\mathbf{r}_b)\chi^-(\mathbf{K}_b,\mathbf{r}_a)|1/r_{ab}|\chi^+(\mathbf{K}_0,\mathbf{r}_a)\psi_{nlm}(\mathbf{r}_b)\rangle . \quad (2b)$$

In (2) ψ_{nlm} is the initial bound-state wave function and χ^+ and χ^- are distorted waves for the initial and final electrons, respectively, with outgoing (+) and ingoing (−) scattered wave boundary conditions. The orbitals ψ_{nlm} have been taken from the Hartree-Fock tables of Clementi and Roetti [35] for neutral atoms. The incoming distorted wave χ^+ has been calculated in the static-exchange potential of the neutral Xe atom. For the outgoing distorted waves χ^-, two possibilities have been considered:

(a) The wave function $\chi^-(\mathbf{K}_a,\mathbf{r})$ for the fast scattered electron has been calculated in the static-exchange potential of the neutral atom, while that for the slow ejected electron $\chi^-(\mathbf{K}_b,\mathbf{r})$ has been evaluated in the spherically averaged spin-singlet static-exchange potential of the final ion state.

(b) Both the outgoing wave functions $\chi^-(\mathbf{K}_a,\mathbf{r})$ and $\chi^-(\mathbf{K}_b,\mathbf{r})$ have been calculated in the spherically averaged spin-singlet static potential of the final ion state.

In both cases each χ^- is orthogonalized to the bound orbital ψ_{nlm}. For asymmetric geometry, such as that considered here, (a), in which the slow ejected electron totally screens the ion charge, makes the best physical sense. However, it has been observed that (b) often gives better agreement with the experiment; this is discussed in Ref. [36]. In the static-exchange calculations of χ^+ and χ^- the local potential of Furness and McCarthy [37], as corrected by Ryley and Truhlar [38], has been used (see Eq. (8) of Ref. [38]).

IV. RESULTS AND DISCUSSIONS

A. Xe 4*d* ionization

The experimental results for the 4*d* ionization at $E_b=20$ and 100 eV are reported in Figs. 3 and 4, respec-

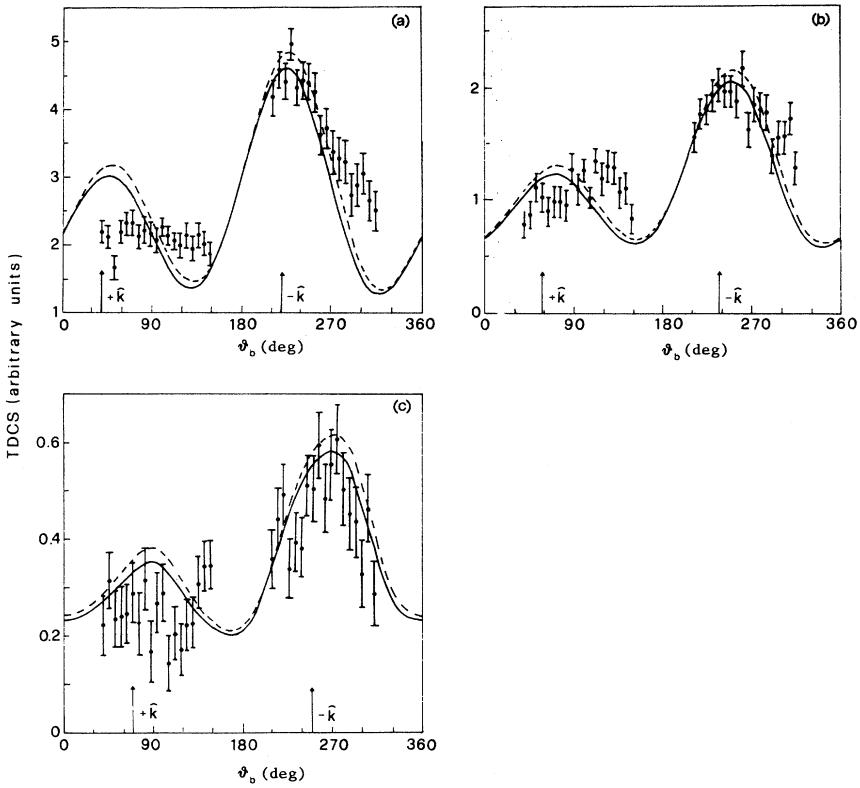

FIG. 3. Relative triple-differential cross sections of Xe $4d$ at $E_a=1000$ eV, $E_b=20$ eV, and $\vartheta_a=2°$ ($K=0.5$ a.u.) (a), 4° ($K=0.7$ a.u.) (b),and 7.5° ($K=1.2$ a.u.). The solid and dashed lines are DWBA calculations with the scattered-electron wave function calculated in the target or in the ion potential, respectively.

tively. The main feature of these TDCS's is the appearance of a large recoil lobe, which is always bigger than the binary peak. The development of a large structure in the recoil direction is usually considered as evidence of final-state interaction of the slow electron with the nucleus. This interaction removes intensity from the forward (binary lobe) to the backward direction.

Let us consider first the measurements with $E_b=20$ eV. Here we have investigated the region of momentum transfer from $K=0.5$ a.u. ($\vartheta_a=2°$) up to $K=1.2$ a.u. ($\vartheta_a=7.5°$), where the kinematics fulfill the Bethe ridge condition. We observe that as K varies, the binary lobe changes shape, becoming a broad feature at $\vartheta_a=2°$ [Fig. 3(a)]. By contrast, there is a well-defined recoil maximum at all three angles. The peak of this maximum lies at a value of ϑ_b larger than that corresponding to the direction $-\mathbf{K}$. These observations are broadly consistent with the findings of previous investigations of inner-shell ionization [6–9].

At $E_b=100$ eV the data for $\vartheta_a=8°$ [Fig. 4(b)] give a binary lobe minimum in the direction of $+\mathbf{K}$ and a recoil lobe maximum in the direction of $-\mathbf{K}$. The data at $\vartheta_a=2°$ [Fig. 4(a)] suggest a similar pattern, but unfortunately the experimental points do not cover a sufficiently large region of ϑ_b to establish the trend. There are three important mechanisms that are relevant to the above observations: (i) competition between direct and resonant ionization, (ii) double scattering effects, and (iii) final-state interaction between the scattered and ejected electrons and the charged decay products of the inner-shell hole.

(i) In $(e,2e)$ measurements on the inner shell $1s$ of C in the molecule C_2H_2, Avaldi, Camilloni, and Stefani [7] have outlined the importance of a resonant channel competing with direct ionization. In order to better investigate this effect in the TDCS without interference from other processes that arise in inner-shell ionization, Avaldi *et al.* [11] have also recently performed an experiment on the $3\sigma_g$ valence orbital of N_2. These latter measurements provide further evidence that the shape of the TDCS is changed when a resonant channel, which can delay the emission of the ejected electron, contributes to the ionization. In particular, a bending of the recoil lobe towards larger ϑ_b was observed. At 20 eV above the $4d$ ionization potential both the electron-energy-loss experiments (Fig. 1) and the photoabsorption measurements show a strong enhancement of the $4d$ cross section. This large increase of the cross section is attributed to a shape resonance in the channel $4d \Longrightarrow \varepsilon f$. The resonance has been also observed to affect the β parameter of the photoelectron angular distribution [39,40], which displays an oscillatory behavior in the region from threshold up to about 100 eV. In the present $(e,2e)$ case one must therefore expect that the resonant channel plays some role in determining the shape of the TDCS.

(ii) Recently Bickert *et al.* [8,9] have studied ionization of Ar($2s$) and Ar($2p$) in a range of coplanar kinematics extending from symmetric geometry ($E_a=E_b=1500$ eV) to very asymmetric geometry ($E_b=150$ eV, $E_a=1500$ eV). They have interpreted their observations in terms of a double binary scattering mechanism [8,41] involving elastic collision of the incident electron with the atom

prior to ionization and elastic collision of the fast scattered electron with the residual ion after ionization. A simple model, which includes these double-scattering effects, qualitatively describes the shape of the recoil lobe measured by Bickert *et al.* [8]; it also describes some features seen in the recoil peak for ionization of Ar($3s$) and Ar($3p$) in asymmetric kinematics with $E_a = 1500$ eV and $E_b = 40$ eV [42].

(iii) A further contribution to the observed shape of the $4d$ TDCS may come from the final-state interaction of the slow ejected electron and the Auger electrons emitted in the decay of the $4d$ hole. This post-collision interaction (PCI) will lead to an exchange of energy and angular momentum between the two electrons [43,44]. Recent theoretical models predict a dependence of the Auger line shape on the mutual angle of the ejected and Auger electrons. The effect is enhanced when the emerging particles have nearly the same velocity. A large fraction of Auger decay channels for the $4d$ vacancy are concentrated in the kinetic-energy region between 15 and 30 eV. Thus a large interaction with the 20-eV ejected electron may occur. So far there exist no predictions of the $(e,2e)$ angular distribution which take account for the (averaged) PCI with the undetected Auger electron. However, Stefani *et al.* [45], in their experimental investigation of the Ar($2p$) ionization, observed that both the $(e,2e)$ and $(e,e'$ Auger) angular distributions bear information on PCI.

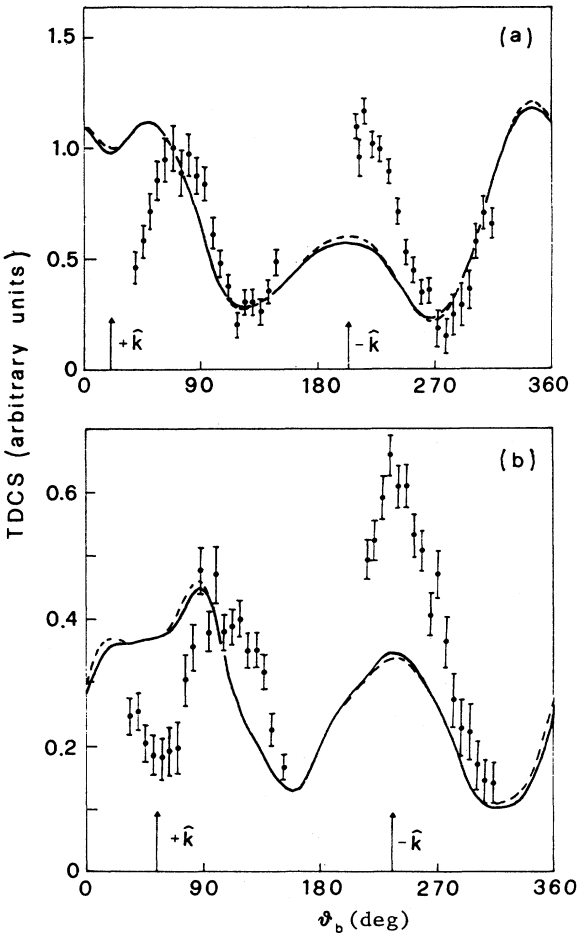

FIG. 4. Relative triple-differential cross sections of Xe $4d$ at $E_a = 1000$ eV, $E_b = 100$ eV, and $\vartheta_a = 2°$ ($K = 0.76$ a.u.) (a) and 8° ($K = 1.4$ a.u.) (b). The solid and dashed lines are DWBA calculations with the scattered-electron wave function calculated in the target or in the ion potential, respectively.

We turn now to the comparison between the DWBA calculations and experiment. We first note that our DWBA approximation will automatically take account of the $4d \Longrightarrow \varepsilon f$ shape resonance of (i) and the double-scattering mechanism of (ii). How well the resonance is represented will depend upon how good our static-exchange approximation with local exchange potential is. The double-scattering mechanisms (ii) are also implicit in the DWBA approximation—elastic scattering of the incident electron by the atom prior to ionization is taken into account through the distorted-wave χ^+, while elastic scattering of the final-state electrons is also incorporated through the distorted waves χ^-. Interaction between the ejected electron and the Auger electron from decay of the $4d$ hole, (iii), is, of course, not described by our DWBA approximation. As mentioned in Sec. III, we have performed two sets of calculations. In the first set the wave function of the scattered electron is calculated in the static-exchange potential of the neutral target atom [case (a)], in the second set it is calculated in the spherically averaged spin-singlet static-exchange potential of the final ion state [case (b)]. Both calculations are shown in our figures (3–6) and for both $4d$ and $5p$ ionization they differ little from one another. The experimental data, which are relative, have been normalized to the case (a) calculation as indicated in Table I. Note that there is only one normalization for each ejected-electron energy, since for fixed ejected energy the relative normalization of the data at different ϑ_a is determined by the experiment.

For $E_b = 20$ eV, Fig. 3, there is quite good, although not perfect, agreement with experiment in the region of the recoil peak. The smaller binary peak is, however, not well described by the calculation, particularly with decreasing momentum transfer K. For $E_b = 100$ eV, Fig. 4, the best that can be said is that the theory predicts dips and bumps more or less where they are observed in the experiment but fails to get the relative size of these structures correctly.

B. Xe $5p$ ionization

The results of our measurements on $5p$ ionization at $E_b = 20$ and 80 eV are shown in Figs. 5 and 6, respectively. At $E_b = 20$ eV our two choices of the angle ϑ_a, namely 2.5° and 8°, correspond to the minimum momentum transfer K (0.4 a.u.) which we can reach with our apparatus (i.e., the closest we can approach the dipole limit) and to Bethe ridge kinematics (i.e., impulsive regime), respectively. At the smaller K, Fig. 5(a), the TDCS displays two lobes which are not symmetric around **K**, but are bent in a way to reduce the relative angle between them. This feature is common to several $(e,2e)$ experiments at similar incident energy and momentum transfer [2], and has always been interpreted as a sign of higher-

order effects in the scattering dynamics. The data on the Bethe ridge, Fig. 5(b), are characterized by a split binary lobe, typical of experiments which probe the region of small momenta of a p-orbital wave function. At 20 eV above threshold, however, the ionization cannot be represented by a pure two-body binary collision, in which the interaction of the ejected electron with the residual ion is neglected. This is clearly shown by the nonvanishing coincidence yield in the backward direction which comes from recoil off the ion. No appreciable shift of the symmetry of the experimental TDCS from the direction of **K** has been observed in this kinematics.

For $E_b=20$ eV and $\vartheta_a=2.5°$, Fig. 5(a), the DWBA predicts a TDCS which is close to symmetric about the direction of **K** if the distorted wave function of the scattered electron is calculated in the potential of the neutral target [case (a)]. However, if the ion potential is used to calculate the same wave function, then the symmetry axis of the resultant TDCS is shifted by about 4° with respect to the direction of **K**. This brings the calculation into marginally better agreement with experiment in the binary lobe. While the DWBA cross section is in general agreement with the measurements at $\vartheta_a=2.5°$, it clearly fails to describe the shift of the experimental peaks away from the direction of **K** and underestimates the binary-to-recoil ratio by about 30%. This is consistent with previous results on He [36] and confirms that the DWBA needs to be improved by including long-range electron-electron interaction in the final state. In the Bethe ridge kinematics, Fig. 6(b), the DWBA correctly describes the binary peak and details well the shape of the recoil peak, although the binary-to-recoil ratio is still a little bit lower than that indicated by experiment.

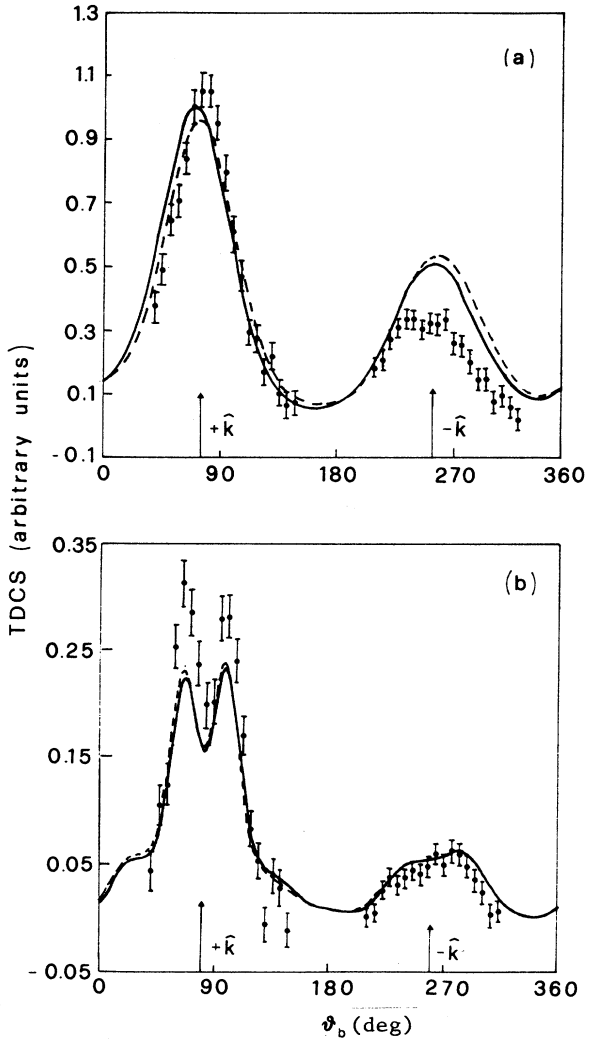

FIG. 5. Relative triple-differential cross sections of Xe $5p$ at $E_a=1000$ eV, $E_b=20$ eV, and $\vartheta_a=2.5°$ ($K=0.40$ a.u.) (a) and 8° ($K=1.2$ a.u.) (b). The solid and dashed lines are DWBA calculations with the scattered-electron wave function calculated in the target or in the ion potential, respectively.

The comparison between the DWBA calculations and experiment at $E_b=80$ eV, Fig. 6, shows that while good agreement between theory and experiment exists at the larger K, Figs. 6(c) and 6(d), there is a rapid deterioration in accord as K decreases. This is quite surprising because a first-order theory is expected to work better as $K\Longrightarrow 0$; moreover, if the failure of the theory were due to a poor description of the ejected-electron wave function, one might expect that the same disagreement would exist at all ϑ_a's investigated. The large recoil lobe observed at $\vartheta_a=1.5°$, with an intensity almost equal to the binary one, is a feature that cannot be explained on the basis of previous $(e,2e)$ works on the outer shell. Indeed, the K value of this kinematics (0.45 a.u.) is almost the same as that corresponding to $E_b=20$ eV and $\vartheta_a=2.5°$. In that case the ratio of the binary-to-recoil intensity is about 2.7, and as E_b increases this ratio is not expected to increase. Ratios which approach unity have been observed in He either upon highly asymmetric kinematics at incident energy of several KeV and vanishing K or near threshold. Both the mentioned conditions are quite far from the ones of the present experiment.

On the other hand, the energy loss for $E_b=80$ eV ($\Delta E\cong 90$ eV) corresponds to the ΔE needed to excite the shape resonance in the $4d$ channel. Many-body photoionization calculations [46–48] and photoelectron spectroscopy measurements [39,49–51] have demonstrated that the outer-shell ($5p$ and $5s$) photoemission processes are affected by strong electron-correlation interactions with the $4d$ subshell in the energy region of the $4d$ threshold and in the region of the shape resonance. In this process the $4d$ subshell undergoes a virtual photoexcitation with the excitation passing to the $5p$ subshell via Coulomb interaction. This coupling produces an enhancement of the $5p$ and $5s$ partial cross section as well as oscillations in the $5p$ β parameter, which could be explained only by models that account for intershell correlations. It is therefore to be expected that such intershell coupling will also be important in $(e,2e)$ collisions at small K, which is close to the photoionization dipolar region. Since $4d$ ionization results in large recoil lobes, Figs. 3 and 4, we speculate that coupling between the $5p$ and $4d$ shells may explain the large recoil yield in the $5p$ TDCS.

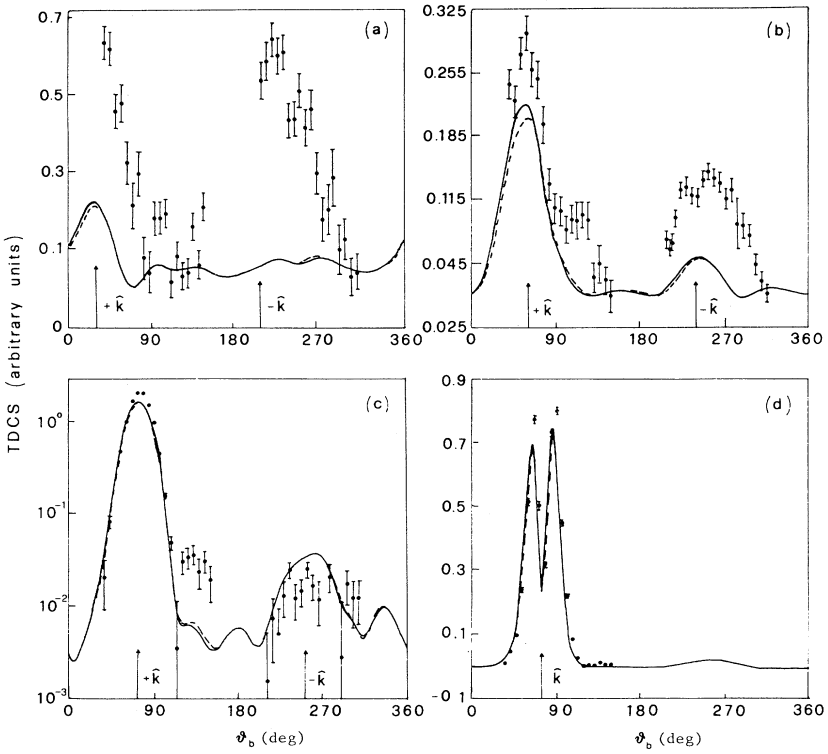

FIG. 6. Relative triple-differential cross sections of Xe $5p$ at $E_a = 1000$ eV, $E_b = 80$ eV, and $\vartheta_a = 1.5°$ ($K = 0.45$ a.u.) (a), 5° ($K = 0.9$ a.u.) (b), 12° ($K = 1.9$) (c), and 15.5° ($K = 2.4$ a.u.) (d). The solid and dashed lines are DWBA calculations with the scattered-electron wave function calculated in the target or in the ion potential, respectively.

V. CONCLUSIONS

Measurements of relative $(e,2e)$ triple-differential cross sections have been made for ionization of the $4d$ and $5p$ shells of Xe at an incident energy of about 1000 eV. The $4d$ measurements extend the rather limited body of experimental data presently available on the inner shell. Calculations in the distorted-wave Born approximation (DWBA) using distorted waves generated in the static-exchange potentials of the atom or resultant ion have been made to compare with the data.

For $4d$ ionization there is reasonable, although by no means perfect, agreement between experiment and theory at the lower ejection energy $E_b = 20$ eV. At the higher energy, $E_b = 100$ eV, agreement is much worse, although the general pattern of dips and bumps in the experimental cross section is mimicked by the theory. The theory, it should be noted, does include a double-scattering mechanism and ionization via the resonant channel $4d \Longrightarrow \varepsilon f$, which are considered to be important.

For $5p$ ionization at $E_b = 20$ eV the agreement between the DWBA and experiment is relatively good, the difference between the two originating as expected from a first-order theory that neglects the interaction between the scattered and ejected electrons. For $E_b = 80$ eV, however, while there is good accord at the larger values of momentum transfer K, there is rapid deterioration as K is reduced.

The disagreements observed between the DWBA calculations and experiment, both for $4d$ and $5p$ ionization, suggest that the theory be improved in a number of ways. First, it is desirable that the static-exchange distorted waves be calculated with the exact nonlocal exchange potential rather than with local approximations to exchange, as done here. Second, spherical averaging of the ion's static-exchange potential should also be avoided, and the calculations should be carried out with the true nonspherical potential. Third, and most importantly, interchannel coupling between the $4d$ and $5p$ orbitals should be taken into account in calculating the final ionized state of the atom. This coupling is known to be important in photoionization of Xe, but the present measurements, we believe, are the first observation of such an effect in $(e,2e)$ experiments. Fourth, if absolute perfection of agreement between theory and experiment is to be obtained, the interaction between the scattered and ejected electrons also needs to be included. Calculations implementing these ideas have been initiated.

ACKNOWLEDGMENTS

This work was partially supported by the EEC Contract Science M.SCI.*0175-C(EDB) and by the NATO Contract No. C.R.G.920101.

*Permanent address: Department of Physics, University of Texas at Austin, Austin, TX 78712.
†Permanent address: Department of Modern Physics, The University of Science and Technology of China, Anhui, People's Republic of China.

[1] I. E. McCarthy and E. Weigold, Rep. Prog. Phys. **51**, 299 (1988).
[2] H. Ehrhardt, G. Knoth, P. Schlemmer, and K. Jung, Z. Phys. D **1**, 3 (1986).
[3] A. Lahman-Bennani, J. Phys. B **24**, 2401 (1991).
[4] L. Avaldi, R. Camilloni, E. Fainelli, and G. Stefani, J. Phys. B **20**, 4163 (1987).
[5] A. Lahman-Bennani, L. Avaldi, E. Fainelli, and G. Stefani, J. Phys. B **21**, 2145 (1988).
[6] A. Lahman-Bennani, H. F. Wellestein, A. Duguet, and A. Daoud, Phys. Rev. A **30**, 1511 (1984).
[7] L. Avaldi, R. Camilloni, and G. Stefani, Phys. Rev. A **41**, 134 (1990).
[8] P. Bickert, W. Hink, C. Dal Cappello, and A. Lahman-Bennani, J. Phys. B **24**, 4603 (1991).
[9] X. Zhang, C. T. Whelan, H. R. J. Walters, R. J. Allan, P. Bickert, W. Hink, and S. Schonberger, J. Phys. B **25**, 4325 (1992).
[10] L. Avaldi, R. Camilloni, G. C. King, and G. Stefani, Phys. Rev. A **44**, 4740 (1991).
[11] L. Avaldi, R. Camilloni, E. Fainelli, and G. Stefani, J. Phys. B **25**, 3551 (1992).
[12] G. Stefani, L. Avaldi, and R. Camilloni, J. Phys. B **23**, L227 (1990).
[13] C. Dupré, A. Lahmam-Bennani, A. Duguet, F. Mota-Furtado, P. F. O'Mahony, and C. Dal Cappello, J. Phys. B **25**, 259 (1992).
[14] A. Lahmam-Bennani, A. Duguet, C. Dupré, and C. Dal Cappello, J. Electron. Spectrosc. Relat. Phenom. **58**, 17 (1992).
[15] M. O. Krause, in *Synchrotron Radiation Research,* edited by H. Winick and S. Doniach (Plenum, New York, 1980), p. 104.
[16] V. Schmidt, Appl. Opt. **19**, 4080 (1980).
[17] B. Crasemann and F. Wuilleumier, in *Atomic Inner-Shell Physics,* edited by B. Crasemann (Plenum, New York, 1985), p. 281.
[18] J. W. Cooper, Phys. Rev. Lett. **13**, 762 (1964).
[19] J. L. Dehmer, A. F. Starace, U. Fano, J. Sugar, and J. W. Cooper, Phys. Rev. Lett. **26**, 1521 (1971).
[20] U. Becker, D. Szostak, H. G. Kerkhoff, H. Kupsch, B. Langer, R. Wehlitz, A. Yagishita, and T. Hayaishi, Phys. Rev. A **39**, 3902 (1989).
[21] E. Weigold, in *Momentum Wave Functions-1976 (Indiana University),* Proceedings of the Workshop/Seminar on Momentum Wave Function Determination in Atomic, Molecular, and Nuclear Systems, edited by D. W. Devins, AIP Conf. Proc. No. 36 (AIP, New York, 1977); A. Giardini-Guidoni, R. Fantoni, R. Camilloni, and G. Stefani, in *Emission and Scattering Techniques,* edited by P. Day (Reidel, Dordrecht, 1981, p. 293.
[22] V. V. Afrosimov, Yu. S. Gordeev, V. M. Lavrov, and S. G. Shchemelinin, Zh. Eksp. Teor. Fiz. **55**, 1569 (1968) [Sov. Phys. JETP **28**, 821 (1969)].
[23] W. F. Chan, G. Cooper, X. Guo, G. R. Burton, and C. E. Brion, Phys. Rev. A **46**, 149 (1992).
[24] G. C. King, M. Tronc, F. H. Read, and R. C. Bradford, J. Phys. B **10**, 2479 (1977).
[25] X. Zhang, C. J. Whelan, and H. R. J. Walters, Z. Phys. D **23**, 301 (1992).
[26] T. Rosel, K. Jung, H. Ehrhardt, X. Zhang, C. T. Whelan, and H. R. J. Walters, J. Phys. B **23**, L649 (1990).
[27] X. Zhang, C. T. Whelan, and H. R. J. Walters, J. Phys. B **23**, L173 (1990).
[28] L. Avaldi, G. Stefani, I. E. McCarthy, and X. Zhang, J. Phys. B **22**, 3079 (1989).
[29] E. Fainelli, R. Camilloni, G. Petrocelli, and G. Stefani, Nuovo Cimento D **9**, 33 (1987).
[30] G. Stefani, R. Camilloni, and A. Giardini-Guidoni, Phys. Lett. **64A**, 364 (1978).
[31] A. Lahmam-Bennani, H. F. Wellestein, A. Duguet, and M. Lecas, Rev. Sci. Instrum. **56**, 43 (1985).
[32] Y-K. Kim, Phys. Rev. A **28**, 656 (1983).
[33] C. B. Opal, E. C. Beaty, and W. K. Peterson, At. Data Nucl. Data Tables **4**, 209 (1972).
[34] I. E. McCarthy and X. Zhang, J. Phys. B **22**, 2189 (1988).
[35] E. Clementi and C. Roetti, At. Data Nucl. Data Tables **14**, 177 (1974).
[36] L. Avaldi, R. Camilloni, P. Letardi, G. Stefani, I. E. McCarthy, X. Zhang, H. R. J. Walters, and C. T. Whelan, Z. Phys. D **23**, 341 (1992).
[37] J. B. Furness and I. E. McCarthy, J. Phys. B **6**, 2280 (1973).
[38] M. E. Riley and D. G. Truhlar, J. Chem. Phys. **63**, 2182 (1975).
[39] L. Torop, J. Morton, and J. B. West, J. Phys. B **9**, 2035 (1976).
[40] S. H. Soutworth, P. H. Kobrin, C. M. Truesdale, D. Lindle, S. Owaki,and D. A. Shirley, Phys. Rev. A **24**, 2257 (1981).
[41] P. Bickert and W. Hink (unpublished).
[42] L. Avaldi, R. Camilloni, C. Dal Cappello, E. Fainelli, A. Lahmam-Bennani, and G. Stefani, Z. Phys. D **16**, 107 (1990).
[43] P. van der Straten, R. Morgenstein, and A. Niehaus, Z. Phys. D **8**, 35 (1988).
[44] M. Ya. Kuchiev and S. A. Sheinerman, Zh. Eksp. Teor. Fiz. **90**, 1680 (1986).
[45] G. Stefani, L. Avaldi, A. Lahmam-Bennani, and A. Duguet, J. Phys. B **19**, 3781 (1986).
[46] M. Ya. Amusia and V. K. Ivanov, Phys. Lett. **59A**, 194 (1976).
[47] M. Ya. Amusia, Comments At. Mol. Phys. **8**, 61 (1979).
[48] W. R. Johnson and K. T. Cheng, Phys. Rev. **A20**, 978 (1979).
[49] J. B. West, P. R. Woodruff, K. Codling, and R. G. Houlgate, J. Phys. B **9**, 407 (1976).
[50] M. G. White, S. H. Soutworth, P. Kobrin, E. D. Poliakoff, R. A. Rosenberg, and D. A. Shirley, Phys. Rev. Lett. **43**, 1661 (1979); **44**, 620(E) (1980).
[51] M. O. Krause, T. A. Carlson, and P. R. Woodruff, Phys. Rev. A **24**, 1374 (1981).